Soft Matter

Cite this: *Soft Matter*, 2011, **7**, 6255

www.rsc.org/softmatter

PAPER

Synthesis of thermally stable Au-core/Pt-shell nanoparticles and their segregation behavior in diblock copolymer mixtures†

Se Gyu Jang,[a] Anzar Khan,[e] Michael D. Dimitriou,[ac] Bumjoon J. Kim,[f] Nathaniel A. Lynd,[a] Edward J. Kramer*[abc] and Craig J. Hawker*[acd]

Received 10th February 2011, Accepted 5th May 2011
DOI: 10.1039/c1sm05223c

We report a facile strategy for the preparation of sub-5 nm gold/platinum (Au-Pt) nanoparticles which are thermally stabilized by a crosslinked polymer shell. Diblock copolymer (PS-*b*-PI-SH) ligands on the Au nanoparticles were used to crosslink the vinyl functionalities on PI *via* hydrosilylation with 1,1,3,3-tetramethyldisiloxane in the presence of a platinum catalyst. The Pt catalyst was reduced on the Au nanoparticles during the hydrosilylation reaction resulting in the formation of a Pt-shell on the Au nanoparticle. The hydrosilylation reaction on the Au nanoparticles as well as their positioning in films of a poly(styrene-*b*-2-vinylpyridine) (PS-*b*-P2VP) block copolymer were thoroughly characterized by X-ray diffraction (XRD), high-resolution transmission electron microscopy (HR-TEM), UV-VIS spectroscopy, and X-ray photoelectron spectroscopy (XPS). Variables such as number of vinyl groups on PS-*b*-PI-SH ligands, the areal density of these ligands on the Au nanoparticle as well as the concentrations of the reactive species were varied systematically to obtain thermally stable nanoparticles. Au-Pt nanoparticles were stable in organic solvents up to 130 °C, and in polymer films at 190 °C for several days. This increased stability allowed the nanoparticles to be thermally annealed in films of PS-*b*-P2VP where their strong interfacial activity and localization were observed.

Introduction

The spontaneous self-assembly of block copolymers into microphase-separated periodic structures as a templating strategy for the organization of inorganic nanoparticles can provide novel functional composite materials for catalysis, photonic band gap modulation, chemical sensing, and electronic device fabrication.[1–5] Surface modification of the nanoparticles is necessary to avoid nanoparticle aggregation or macrophase separation as well as to control their location within the block copolymer. In the case of an AB diblock copolymer the nanoparticles can be located wholly in the A domain, at the AB interface, or in the B domain. The most promising strategy for controlling location of inorganic nanoparticles is through tailoring their organic-modified surfaces. This approach has been a topic of intensive study,[6–18] focusing recently on the grafting of oligomer- or polymer-ligands to the nanoparticle surface.[19,20] For example, nanoparticles stabilized by various thiol-terminated polymer ligands have been used to precisely control the localization of nanoparticles to one domain or to the interface between domains of diblock copolymers.[11,13,14,21,22] In particular, the formation of desirable bicontinuous phases can be driven by selective segregation of surfactant-like Au nanoparticles to the interface of a lamellar-forming diblock copolymer.[13,23] Au nanoparticles are considered a model inorganic nanoparticle for the study of interactions between nanoparticle ligands and block copolymer domains for the following reasons: Au nanoparticles can be synthesized with diameters that are small compared to the size of block copolymer domains, have high contrast in transmission electron microscopy (TEM), have relatively narrow size-distributions, are easily prepared, and can be functionalized with a variety of ligands. Despite the advantages listed above, a significant challenge is the poor thermal stability of the Au–S bonds which leads to aggregation of the Au nanoparticles at 50–60 °C.[24] This limitation has restricted the use of Au

[a]*Materials Research Laboratory, University of California, Santa Barbara, California, 93106, USA. E-mail: edkramer@mrl.ucsb.edu; hawker@mrl.ucsb.edu*
[b]*Department of Chemical Engineering, University of California, Santa Barbara, California, 93106, USA*
[c]*Department of Materials, University of California, Santa Barbara, California, 93106, USA*
[d]*Department of Chemistry and Biochemistry, University of California, Santa Barbara, California, 93106, USA*
[e]*Department of Materials, Institute of Polymers, ETH-Zürich, Wolfgang-Pauli-Strasse 10, HCl H-520, 8093 Zürich, Switzerland*
[f]*Department of Chemical and Biomolecular Engineering, Korea Advanced Institute of Science and Technology, Daejeon, 305-701, Republic of Korea*

† Electronic supplementary information (ESI) available: ^{1}H-NMR spectra of Au-Pt nanoparticles hydrosilylated with various amount of TMDS (ESI 1, Fig. SF1). TEM micrographs of Au or Au-Pt nanoparticles after thermal stability tests (ESI 2, Fig. SF2). XPS spectrum of Pt obtained from shell-crosslinked Au-Pt nanoparticles and detailed discussion (ESI 3, Fig. SF3). Cross-sectional TEM micrographs of PS_{547}-*b*-$P2VP_{542}$ containing PS_{29}-*b*-I_{21}SAu_4 nanoparticles whose ligands are not crosslinked (ESI 4, Fig. SF4). See DOI: 10.1039/c1sm05223c

nanoparticles, as well as composite materials made with them, to lower temperature environments or processing strategies.

One approach to stabilize self-assembled systems is through crosslinking which has been widely used for the stabilization of assemblies such as micelles and vesicles against thermal or other external stimuli.[25–27] Recently, polymeric nanocapsules for drug-delivery were synthesized by crosslinking the ligands on a nanoparticle template followed by removal of the core.[28,29] Similar crosslinking approaches have been used to synthesize thermally-stable nanoparticles.[30–32] As an example, Dong *et al.* demonstrated a novel method for synthesizing Au nanoparticles with crosslinked shells *via* a one-pot polymerization of both monomer and crosslinker from the surface of the Au nanoparticles.[33] Although the crosslinking of the ligands was successful as evidenced by the stability of the nanoparticles in toluene solution at elevated temperatures (110 °C), the size of the nanoparticles including the polymeric ligand was large due to the thick crosslinked polymer shell (~24 nm). The large size of these nanoparticles rules out their application in cooperative self-assembly with diblock copolymer mesostructures, which would be disrupted by such large nanoparticles. Furthermore, precise control of areal chain densities of ligands on the Au nanoparticles that has been shown to be important in controlling the localization of nanoparticles in diblock copolymer mesophases[22] may be difficult to achieve and the effect of crosslinker itself on the effective Flory-Huggins parameter of the shell is not easy to predict. To improve the controllability of the areal density and length of ligands on Au nanoparticles, the use of diblock copolymer ligands, where one block is crosslinkable, was proposed by Yoo *et al.*[34] In this work, controlled synthesis of small Au nanoparticles (~3 nm in diameter) with a well-defined number of ligands and crosslinking groups showed great potential as a method to incorporate shell-crosslinked nanoparticles in a polymer matrix. For example, the nanoparticles were segregated along the interface of polymethylmethacrylate (PMMA) and PS in binary homopolymer blends after thermal annealing due to presence of the polar groups in the crosslinked shell on the Au nanoparticle. However, the thermal stability of the nanoparticles as a function of the areal chain density (Σ) of ligands, the length of the crosslinkable block related to the size of nanoparticle, and the localization of shell-crosslinked nanoparticles in block copolymer mesophases still remains to be explored.

Here, we report a simple route to prepare sub-5nm diameter thermally stable Au-core/Pt-shell nanoparticles incorporating a crosslinked polymeric shell and the influence of structure on the localization of these core-shell nanoparticles within microphase-separated domains of PS_{547}-*b*-$P2VP_{542}$ diblock copolymers. Inspired by Yoo *et al.*, a thiol-terminated poly(styrene-*b*-1,2&3,4 isoprene) diblock copolymer ligand (PS-*b*-PI-SH) was synthesized by sequential anionic polymerization under conditions favoring the 1,2- and 3,4-regioisomer of polyisoprene. Following the synthesis of Au nanoparticles in the presence of the thiol terminated PS-*b*-PI diblock, the pendant vinyl groups on the PI block were crosslinked *via* a hydrosilylation reaction with 1,1,3,3-tetramethyldisiloxane in the presence of a platinum catalyst.[35] Interestingly, the Pt catalyst used for the hydrosilylation reaction was reduced on the Au nanoparticles during the hydrosilylation reaction resulting in the formation of a Pt-shell on the Au (Au-Pt). The thickness of Pt-shell can be controlled by adjusting the feed of the Pt catalyst. The formation of the Pt-shell was characterized by X-ray diffraction (XRD), high-resolution TEM (HR-TEM), UV-VIS spectroscopy, and X-ray photoelectron spectroscopy (XPS). The thermal stability of the shell-crosslinked Au-Pt nanoparticles was examined by systematic variation of experimental variables such as the length of the crosslinkable block in the ligand, the number of ligands per particle, and the concentration of catalyst and crosslinker. Significantly, the Au-Pt nanoparticles with the crosslinked shell were stable upon heating in organic solvents up to 130 °C as well as in block copolymer films of PS_{547}-*b*-$P2VP_{542}$ annealed in vacuum at 190 °C for several days.

Experimental

Synthesis of PS-*b*-PI-SH by living anionic polymerization

PS-*b*-PI-SH polymers with various lengths of polyisoprene blocks were synthesized by sequential anionic polymerization using tetrahydrofuran (THF) as a solvent at −78 °C as described elsewhere.[12] Briefly, styrene was initiated by *sec*-butyl lithium and was polymerized for three hours under argon. After two hours, a small portion of polystyryl anion was taken with a gas-tight syringe to measure its molar mass by gel permeation chromatography (GPC) calibrated with PS standards. Then, isoprene was added at −78 °C and polymerized for five hours under argon. The polyisoprenyl anions were then titrated with propylene sulfide, and the resulting polymers protonated by acidic methanol and stirred overnight. The M_n values of three different PS-*b*-PI-SH were determined to be 3.8, 4.6, and 7.3 kg mol^{-1} by GPC with the M_n of the 1,2- and 3,4-regioisomer-enriched polyisoprene blocks determined to be 0.8, 1.4, and 3.2 kg mol^{-1} by end-group analysis using proton nuclear magnetic resonance spectroscopy (^{1}H NMR, Bruker, 500 MHz). The M_n and polydispersity index (PDI) of the polymers are shown in Table 1. For convenience, these polymers are labeled as PS_{26}-*b*-I_{12}-SH, PS_{29}-*b*-I_{21}-SH, and PS_{35}-*b*-I_{47}-SH, where the subscripts represent the number average degree of polymerization of the PS and PI blocks.

Synthesis of PS-*b*-PI-coated Au nanoparticles

Au nanoparticles with various areal chain densities (Σ) of PS_{26}-*b*-I_{12}-SH, PS_{29}-*b*-I_{21}-SH, and PS_{35}-*b*-I_{47}-SH (see Table 2) were synthesized *via* a two-phase toluene/water method by varying the

Table 1 Characterization of thiol-terminated poly(styrene-*b*-1,2&3,4-isoprene)

	PS (GPC)		PS-*b*-PI-SH (GPC)		PI (NMR)[a]	
	Mn (kg mol^{-1})	PDI	Mn (kg mol^{-1})	PDI	Mn (kg mol^{-1})	N_v[b]
PS_{26}-*b*-I_{12}SH	2.7	1.33	3.8	1.15	0.8	11
PS_{29}-*b*-I_{21}SH	3.0	1.13	4.6	1.08	1.4	20
PS_{35}-*b*-I_{47}SH	3.6	1.15	7.3	1.09	3.2	43

[a] Obtained from end-group analysis by ^{1}H-NMR. [b] Average number of vinyl groups per chain obtained from the number of 1,2- and 3,4- isoprene groups calculated from the ^{1}H-NMR.

Table 2 Characterization of Au nanoparticles tethered by thiol-terminated diblock copolymer ligands

	D_{core} (nm)[a]	$D_{core+shell}$ (nm)[b]	Σ (#/nm^2)[c]	f[d]	f_c[e]
PS_{26}-*b*-I_{12}SAu_1	2.5 ± 0.4	6.5	1.5	31	50
PS_{26}-*b*-I_{12}SAu_2	2.5 ± 0.5	6.6	1.8	34	50
PS_{29}-*b*-I_{21}SAu_1	3.1 ± 1.0	6.6	0.7	19	50
PS_{29}-*b*-I_{21}SAu_2	2.8 ± 0.7	7.5	1.1	22	43
PS_{29}-*b*-I_{21}SAu_3	2.7 ± 0.5	7.9	1.6	36	43
PS_{29}-*b*-I_{21}SAu_4	2.4 ± 0.5	8.1	2.2	39	37
PS_{35}-*b*-I_{47}SAu	2.8 ± 0.7	10.2	1.6	39	31

[a] Mean diameter obtained from image analysis based on TEM images for at least 300 Au nanoparticles. [b] Mean diameter estimated from density of polymer and Au from TGA. [c] Calculated from TGA analysis and D_{core}. [d] Mean number of chains on one nanoparticle calculated from Σ and D_{core}. [e] Critical mean number of ligands on a Au nanoparticle for brush to mushroom transition estimated from radius of Au core and radius of gyration of PI block.

mole feed ratio of thiol-terminated ligands to the Au precursor.[36] The Au nanoparticles were precipitated in methanol at least three times to remove tetraoctylammonium bromide (TOAB, Sigma-Aldrich). The unbound polymer ligands were removed from the Au nanoparticles by precipitating the nanoparticles in hexane at least five times.

Shell-crosslinking of polyisoprene on Au nanoparticle

Pendant vinyl groups on the polyisoprene block were crosslinked by a hydrosilylation reaction using 1,1,3,3-tetramethyldisiloxane (TMDS, Gelest Inc.) in the presence of chloroplatinic acid hexahydrate (CPA, Sigma-Aldrich).[37] First, the dry Au nanoparticle powder was dispersed in dry THF under argon. Then, a calculated amount of the Pt catalyst (10∼200 mol % relative to vinyl groups) and TMDS dissolved in dry THF (30∼150 mol % relative to vinyl groups) was added under magnetic stirring at room temperature. For example, PS_{29}-*b*-I_{21}SAu_3 was crosslinked with 100 mol % of CPA and 75 mol % of TMDS (150 mol % of hydrosilane) relative to vinyl groups. The dark red color of the Au nanoparticle dispersion turned dark brown after 30 min. The reaction continued for two days under argon. After the reaction was completed, nanoparticles were precipitated in a hexane and methanol mixture (1 : 1 v/v) at least three times.

Preparation of PS_{547}-*b*-$P2VP_{542}$/Au-Pt nanoparticle composites

A calculated amount of Au or Au-Pt nanoparticles were dissolved in a freshly prepared 1 wt% PS_{547}-*b*-$P2VP_{542}$ (114 kg mol^{-1}, Polymer Source. Inc.) block copolymer solution in chloroform to obtain about 4–5% volume fraction of nanoparticles in the polymer/nanoparticle composite including the volume of polymer shell estimated from density of polymer (∼1.05 g cm^{-3}) and Au (∼19.3 g cm^{-3}) and thermal gravimetric analysis (TGA) of Au nanoparticles.[22] Block copolymer/nanoparticle composites were prepared by drop casting the solution of nanoparticles and PS_{547}-*b*-$P2VP_{542}$ block copolymer in chloroform onto a thick Au-coated (∼100 nm) sodium chloride crystal window (Sigma-Aldrich, 2 mm thick). The composites were annealed under high vacuum (∼10^{-8} Torr) at 190 °C for at least three days. For the composite sample with nanoparticles that had no crosslinked shell, solvent annealing using saturated dichloromethane (DCM) vapor at room temperature for at least two days was employed. After annealing of the composite, a thick Au layer (∼100 nm) was deposited on the sample to inhibit infiltration of the epoxy resin (Embed-812, Electron Microscopy Sciences) into the sample during TEM sample preparation. Bulk samples of the composite were embedded into epoxy resin and sliced to a thickness of about 50–70 nm by ultra-microtoming (Leica). The sliced composite samples were exposed to iodine vapor to selectively stain the P2VP domains.

Characterization

The nanoparticles as well as cross-sectional images of composite samples were characterized by transmission electron microscopy (TEM, FEI Tecnai G2 microscope, 200 kV, and FEI Titan FEG for HR-TEM). The size histograms of the Au nanoparticles were determined from at least 300 nanoparticles by image analysis (Image Pro) of TEM micrographs. The mean areal chain density of polymer ligands on the Au nanoparticles was calculated from the total surface area and the weight fraction of Au and polymer ligands determined by TGA. UV-VIS spectra of nanoparticles before and after crosslinking of the polyisoprene-shell were recorded in chloroform with a Shimadzu UV 3101PC spectrometer. X-ray photoelectron spectroscopy data (XPS, Kratos Axis Ultra) and X-ray diffraction (XRD, Rigaku smartlab high-resolution diffractometer) patterns were obtained from a powder of Au nanoparticles on a silicon wafer and glass substrate,

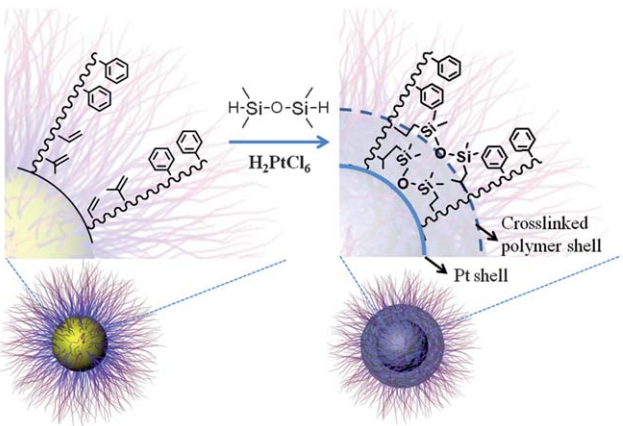

Scheme 1 Schematic illustration of diblock copolymer ligands tethered to the surface of a gold nanoparticle and subsequent crosslinking of the vinyl-rich inner block *via* hydrosilylation with 1,1,3,3-tetramethyldisiloxane in the presence of platinum catalyst. The catalyst undergoes reduction on the gold surface during the reaction and forms a Pt shell.

respectively. XPS measurements were performed using a Kratos Axis Ultra Spectrometer (Kratos Analytical, Manchester, UK) with a monochromatic Al Kα X-ray source (1486.6 eV) operating at 225 W under a vacuum of 1.0×10^{-8} Torr. Charge compensation was carried out by injection of low-energy electrons into the magnetic lens of the electron spectrometer. The pass energy of the analyzer was set at 20 eV for high-resolution spectra with an energy resolution of 0.05 eV. The spectra were analyzed using CasaXPS v.2.3.14 software. The C–C peak at 285 eV was used as the reference for binding energy calibration.

Results and discussion

Scheme 1 illustrates our strategy for shell-crosslinking the Au nanoparticle. PS-*b*-PI-SH was synthesized by sequential anionic polymerization of styrene and isoprene monomers with the polymerization of isoprene performed in THF to produce primarily 1,2- and 3,4-addition of isoprene monomers (>95%) rather than 1,4-addition (<5%).[38] As a result, Au nanoparticles synthesized with diblock copolymer ligands consist of a vinyl-rich PI shell near the surface of the Au and a PS outer brush. The outer PS brush layer inhibits inter-particle crosslinking and stabilizes the nanoparticles in organic solvents. Crosslinking of the PI shell was then achieved by hydrosilylation between the vinyl groups on PI and the hydrosilane functionalities of 1,1,3,3-tetramethyldisiloxane (TMDS) in the presence of a Pt catalyst. Although there are many types of crosslinking reactions that may be used, the variety of chemical reactions that may be carried out on the Au nanoparticles are significantly restricted due to the instability of the gold-sulfur (Au–S) bond. For example, radical crosslinking of vinyl groups or thiol-ene click-chemistry[39] resulted in the detachment of ligands from the Au nanoparticle surface due to the formation of thio-radicals.[40] In contrast, hydrosilylation, which takes place without the formation of radicals was chosen for the crosslinking of the vinyl groups on PI.[35,37,41] Traditionally, a drawback to the hydrosilylation reaction is the formation of Pt colloids (typically 2∼60 nm in diameter) at the beginning of the reaction during the induction period.[42] Interestingly, Pt nanoparticle formation was not observed in the present hydrosilylation reaction on Au nanoparticles. Instead, the Pt catalyst used in the reaction was reduced on the Au nanoparticle surface to produce a thin Pt-shell. This ability to prepare shell-crosslinked Au nanoparticles with a thin Pt-shell in a one-pot reaction is novel and may be potentially useful in catalysis (*e.g.*, the oxidation of CO to CO_2). Detailed characterization of the Pt-shell will be provided in a later section.

For a range of compositions, the crosslinked block copolymer-shell was shown to afford nanoparticle thermal stability at elevated temperatures, however, no systematic investigation of the thermal stability of nanoparticles according to the areal chain density (Σ) and the length of the crosslinkable block has been described. In order to understand the structural parameters required for thermal stability, the mean number of vinyl groups on the ligands (N_v) and the mean number of chains on one nanoparticle (f) were varied. To accomplish this, PS-*b*-PI-SH diblock copolymer ligands with a fixed length of PS (∼3 kg mol^{-1}), but with varied lengths of the vinyl-rich PI ranging from 0.8 to 3.2 kg mol^{-1} as listed in Table 1 were prepared. Molecular weight M_n and corresponding average number of vinyl groups on a PI ligand were obtained from end-group analysis by ^{1}H-NMR. From this library of block copolymer ligands, Au nanoparticles at various f were synthesized (see Table 2) to investigate the effect of f on thermal stability. In Table 2, the mean diameters of Au or Au-Pt cores (D_{core}) were obtained from image analysis of TEM micrographs for at least 300 nanoparticles and the mean diameters of core-shell ($D_{core+shell}$) were estimated based on the density of polymer and Au from TGA. Σ was calculated from D_{core} and the mass ratio of polymer to Au obtained from TGA. The Σ was used to calculate f.

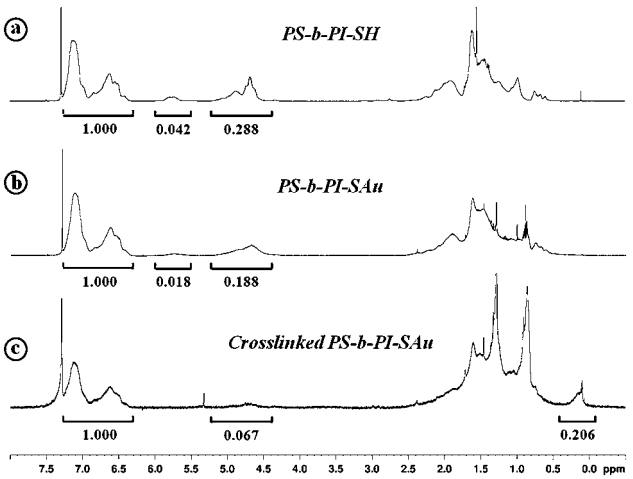

Fig. 1 ^{1}H-NMR spectra of (a) PS_{29}-*b*-I_{21}SH, (b) gold nanoparticles coated by PS_{29}-*b*-I_{21}SH, (c) gold nanoparticles after crosslinking reaction of ligand.

Fig. 1a–c show ^{1}H-NMR spectra of a representative thiol-terminated diblock copolymer ligand in $CDCl_3$ as it goes from being a free ligand in solution, to being localized on a Au nanoparticle surface, followed by crosslinking. Fig. 1a shows the spectrum of the PS_{29}-*b*-I_{21}-SH in solution. Fig. 1b shows the spectrum from Au nanoparticles with attached PS_{29}-*b*-I_{21}-SH ligands (PS_{29}-*b*-I_{21}SAu_3 in Table 2), and finally in Fig. 1c the spectrum from shell-crosslinked Au-Pt nanoparticles after hydrosilylation (shell-crosslinked PS_{29}-*b*-I_{21}SAu_3) are shown. In Fig. 1a, the integration ratio ($\alpha_{C=C}$) of the sum of vinyl peaks centered at 4.7 and 5.7 ppm to the aromatic peaks of PS at 6.3–7.4 ppm yielded 0.33. The ratio $\alpha_{C=C}$ of the same diblock copolymer ligands on the Au nanoparticles was reduced to about 0.21 as shown in Fig. 1b. This decrease in $\alpha_{C=C}$ was due to the restricted mobility of protons densely packed near the surface of a Au nanoparticle and the corresponding spin–spin relaxation (T_2) broadening.[43,44] After the crosslinking reaction was completed, $\alpha_{C=C}$ was reduced from 0.21 to 0.07 due to both consumption of vinyl groups during the hydrosilylation and the further decrease in mobility caused by crosslinking. In addition, new peaks centered at 0.17, 0.87 and 1.34 ppm, corresponding respectively to the protons on Si–C***H***$_3$, Si–C***H***$_2$, and $SiCH_2C\boldsymbol{H}CH_3$ or $SiCH_2C\boldsymbol{H}_2$, are evidence that the PI crosslinking reaction with TMDS was successful. Experimental variables such as the amount of crosslinker and Pt-catalyst relative to the vinyl groups on PI were varied in order to minimize $\alpha_{C=C}$, and these optimal conditions were used to crosslink nanoparticles with various N_v and f. (Fig. SF1, ESI†)

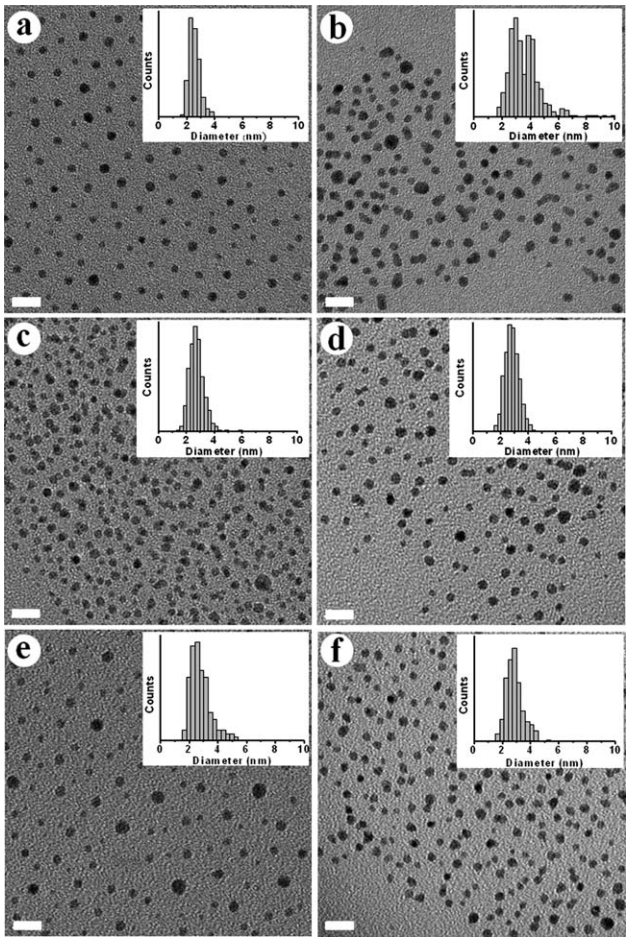

Fig. 2 TEM images showing Au nanoparticles before and after a thermal stability test. (a) PS_{26}-*b*-I_{12}SAu_1, (c) PS_{29}-*b*-I_{21}SAu_3, and (e) PS_{35}-*b*-I_{47}SAu are Au nanoparticles with various lengths of isoprene blocks of 0.8, 1.4, and 3.2 kg mol^{-1}, respectively. Images were taken before crosslinking reaction. (b), (d), and (f) are TEM images of nanoparticles in (a), (c), and (e), respectively, after crosslinking and thermal stability test. Thermal stability tests were conducted by heating a closed ampule containing nanoparticles in toluene for 1 day at 130 °C. Histograms in the insets show size distributions of nanoparticles. Scale bars are 10nm.

In order to examine the effect of N_v on the thermal stability of the shell-crosslinked Au-Pt nanoparticles, three different Au nanoparticles with various $N_v = 11$, 20, and 43 but with similar f (~35 ligands/particle) and PS molar masses (~3 kg mol^{-1}) were prepared. Fig. 2a, c, and e are the respective TEM micrographs of PS_{26}-*b*-I_{12}SAu_1 ($N_v = 11$), PS_{29}-*b*-I_{21}SAu_3 ($N_v = 20$), and PS_{35}-*b*-I_{47}SAu ($N_v = 43$) before crosslinking. The PI shell of the nanoparticles was crosslinked under the previously-determined optimal conditions with the ratio $\alpha_{C=C}$ being less than 0.07 for all nanoparticles after crosslinking. To test the stability of the crosslinked shell around the Au-Pt nanoparticles at elevated temperature, nanoparticle solutions in toluene were sealed in glass ampules and annealed at 130 °C for one day. The respective TEM micrographs of shell-crosslinked PS_{26}-*b*-I_{12}SAu_1 ($N_v = 11$), PS_{29}-*b*-I_{21}SAu_3 ($N_v = 20$), and PS_{35}-*b*-I_{47}SAu ($N_v = 43$) after heating are shown in Fig. 2b, d, and f. Histograms obtained from the averaging over at least 300 nanoparticles for each sample are shown in the insets of each figure and reflect the size distribution of the nanoparticles. Notably, the nanoparticle cores in Fig. 2b grew significantly in mean diameter from 2.5 ± 0.4 nm to 3.6 ± 1.2 nm after the thermal stability test. In principle two main mechanisms of coarsening of the gold nanoparticles, are possible, Ostwald ripening and coalescence. Ostwald ripening occurs by transfer gold atoms through the solvent medium from smaller nanoparticles to larger ones to reduce the total surface energy of nanoparticles.[45,46] In our thermal stability test conditions, Ostwald ripening should be significantly hindered because of the very low solubility of gold atoms in toluene and the absence of free ligands with thiol-ends that might facilitate solubilization of gold atoms in the organic solvent. Therefore, it is likely that coalescence is the primary mechanism of coarsening, a hypothesis supported by the close pairs of partially fused particles in Fig. 2b. Because the Au nanoparticles without crosslinking were precipitated as bulk particles during the same thermal stability test (Fig. SF2a, ESI†), we believe the nanoparticles with PS_{26}-*b*- I_{12}SH were stabilized due to crosslinking, but this crosslinking was not sufficient to completely inhibit the aggregation of nanoparticles. The thermal stability of shell-crosslinked Au-Pt nanoparticles (PS_{26}-*b*-I_{12}SAu_2) synthesized with the same ligand but higher mean number of ligands on a nanoparticle ($f = 34$) was also unsatisfactory (Fig. SF2b, ESI†). From these studies, it can be concluded that the nanoparticles covered by the ligands with only 11 vinyl groups per chain are not stable at elevated temperature. In comparison, shell-crosslinked Au-Pt nanoparticles with longer PI blocks (PS_{29}-*b*-I_{21}SAu_3, $N_v = 20$, $f = 36$) in Fig. 2d showed excellent thermal stability with essentially no difference in mean diameters of nanoparticles before and after thermal aging ($\Delta D_{core} \sim 0$ nm, Fig. 2d). Au-Pt nanoparticles with ligands having more than 20 vinyl groups (PS_{35}-*b*-I_{47}SAu, $N_v = 43$, $f = 39$) also showed satisfactory stability after the thermal stability test (Fig. 2f, $\Delta D_{core} \sim 0$ nm). This observation indicates that thermally stable Au-Pt nanoparticles can be obtained with ligands having more than 20 vinyl groups under these hydrosilylation crosslinking conditions.

The instability of PS_{26}-*b*-I_{12}SAu_1 and PS_{26}-*b*-I_{12}SAu_2 can be ascribed to the short length of PI, equivalent to about 5 Kuhn segments based on the Kuhn segment length of vinyl-rich PI (0.59 nm).[47] The short length of the polymer chain (or oligomer) with only 5 Kuhn segments is expected to limit the conformational freedom of the chain significantly and results in low intermolecular crosslinking of the ligands. Alternative strategies for inducing nanoparticle stability include the use of a longer crosslinking agent, higher f, or more efficient cross-linking chemistry.

The relation of the mean number of chains on one nanoparticle (f) relative to Σ is also an important factor in determining the thermal stability of these shell-crosslinked nanoparticles. To address the effect of f on the thermal stability of nanoparticles, we synthesized three different nanoparticles having f of 19, 22, and 39 with PS_{29}-*b*-I_{21}-SH ($N_v = 20$), as listed in Table 2. Fig. 3a, c, and e are the respective TEM micrographs of PS_{29}-*b*-I_{21}SAu_1 ($f \sim 19$), PS_{29}-*b*-I_{21}SAu_2 ($f \sim 22$), and PS_{29}-*b*-I_{21}SAu_4 ($f \sim 39$) taken before hydrosilylation reaction was carried out. Note that PS_{29}-*b*-I_{21}SAu_3 ($f \sim 36$) was determined to be thermally stable in the previous experiment. After crosslinking and thermal stability testing, the nanoparticles were characterized by TEM with the ΔD_{core} being 0.7, 0.4, and 0 nm for the particles shown in Fig. 3b,

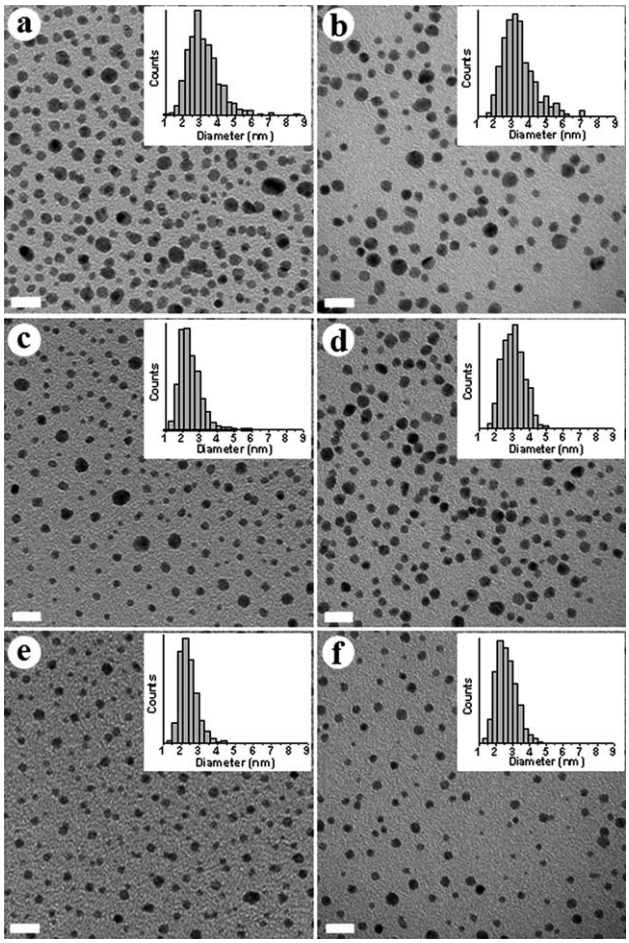

Fig. 3 TEM micrographs showing Au nanoparticles before and after thermal stability testing. (a) PS_{29}-*b*-I_{21}SAu_1 (f = 19), (c) PS_{29}-*b*-I_{21}SAu_2 (f = 22), and (e) PS_{29}-*b*-I_{21}SAu_3 (f = 39) are TEM images of Au nanoparticles taken before the crosslinking reaction, where f is the mean number of ligands on a nanoparticle. (b), (d), and (f) are TEM images of nanoparticles taken after crosslinking and the thermal stability test of the nanoparticles in (a), (c), and (e), respectively. Histograms in the insets show the size distribution of nanoparticles. Scale bars are 10 nm.

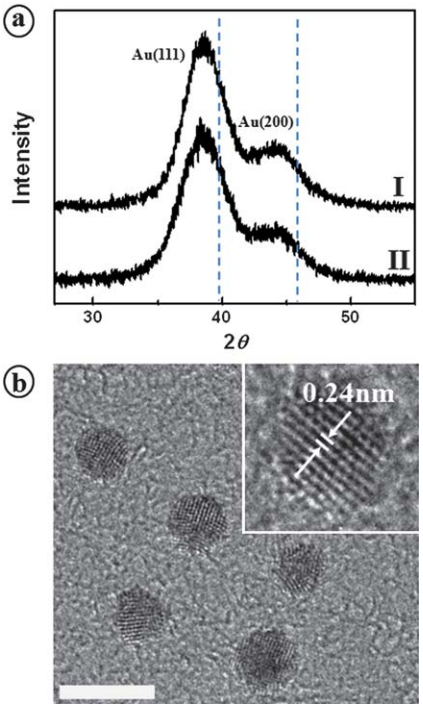

Fig. 4 Characterization of shell-crosslinked Au-Pt nanoparticles. (a) XRD spectra of Au nanoparticles (I) before and (II) after crosslinking reaction showing similar crystallinity. Peaks at $2\theta = 38.2°$ and 44.4° correspond to the Au (111) and Au (200) crystal planes, respectively. Dashed lines at $2\theta = 39.8°$ and 46.2° show the reported peak positions of Pt (111) and Pt (200), respectively. (b) HR-TEM image of shell-crosslinked gold nanoparticles. Scale bar is 5 nm. Inset is magnified image showing the (111) lattice planes of gold nanoparticle observed with a lattice spacing of ~0.24nm.

d, and f, respectively. The increased thermal stability of the Au-Pt nanoparticles with higher f can be explained by the conformation of polymeric ligands on the nanoparticle. Polymeric ligands on Au nanoparticles have mushroom conformations when f is lower than the critical f for the brush to mushroom transition (f_c). Larger f results in more chain stretching in the mushroom conformation and larger intermolecular contact area of ligands. Consider a particle of radius R_{core} with f ligands bound on the core, each with a radius of gyration of PI ($R_{g,\ PI}$). The f_c can be roughly estimated according to eqn (1).

$$f_c \approx 4\pi \times 0.68 \times \left(\frac{R_{core} + R_{g,PI}}{R_{g,PI}}\right)^2 \quad (1)$$

The prefactor in eqn (1) was adapted from the empirical results by Kim *et al.*[21] The estimated f_c values for each nanoparticle are listed in Table 2. If f is significantly lower than f_c, almost no intermolecular crosslinking is expected to occur. Therefore, the thermal instability of PS_{29}-*b*-I_{21}SAu_1 and PS_{29}-*b*-I_{21}SAu_2 is attributed to the much lower values of f than f_c. From our results, certain N_v and f values were required to obtain a stable crosslinked shell at elevated temperatures, specifically $N_v > 20$ and $f > 36$ (PS_{29}-*b*-I_{21}SAu_3). We emphasize that the N_v and f values above are also dependent on the crosslinking method or yield of crosslinking reaction, length of the crosslinker, and the size of nanoparticle core which determines the curvature of the core and directly affects the density of ligands near the core surface.

It is well known that the Pt catalyst used in hydrosilylation can form Pt nanoparticles during the initial stages of the reaction where it may lead to a mixture of Pt and Au nanoparticles in our crosslinking system.[42] To investigate the presence of Pt nanoparticles, nanoparticle powders were characterized by X-ray diffraction (XRD) with the diffraction patterns obtained before and after hydrosilylation of PS_{29}-*b*-I_{21}SAu_4 shown in Fig. 4a. In both cases, peak positions are located at $2\theta = 38.2°$ and 44.4° where exactly matches with the reference values for the Au (111) and Au (200) lattice planes. Blue dotted lines in Fig. 4a indicate the expected peak positions of $2\theta = 39.8°$ and 46.2° for Pt (111) and (200), respectively. In the case of a physical mixture of Au and Pt nanoparticles, the Pt (111) and (200) peaks should be observed together with peaks corresponding to the Au nanoparticle. From these results, it can be concluded that the hydrosilylation produces neither Au/Pt alloy nanoparticles nor crystalline Pt nanoparticles. Although the broad peaks are

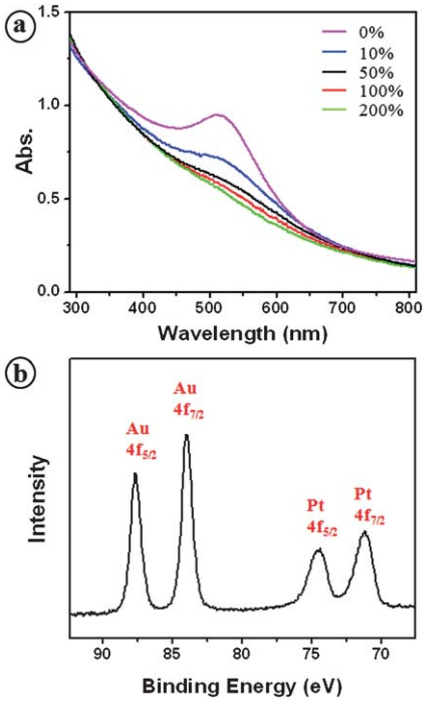

Fig. 5 Characterization of shell-crosslinked Au-Pt nanoparticles. (a) UV-VIS spectra of Au nanoparticles hydrosilylated with various mol % of Pt catalyst relative to the vinyl groups on the nanoparticle. (b) $4f_{5/2}$ and $4f_{7/2}$ XPS spectra of Au and Pt obtained from shell-crosslinked Au-Pt nanoparticles.

consistent with the small size of the nanoparticles, there is no difference between the two diffraction patterns and no evidence of crystalline Pt nanoparticles. In contrast, the diffraction peaks for bimetallic Au/Pt alloys should appear as single peaks between the pure Au and Pt lattice plane peaks.[48] In addition, we clearly observe only the lattice planes of the Au nanoparticles using high-resolution transmission electron microscopy (HR-TEM) as shown in Fig. 4b.

Fig. 5a shows UV-VIS absorption spectra for a set of shell-crosslinked Au-Pt nanoparticles (PS_{29}-*b*-I_{21}SAu_3) hydrosilylated with 0 to 200 mol % of Pt catalyst relative to vinyl groups. Significantly, the surface plasmon resonance peak (SPR)[49] of the Au nanoparticles near 520 nm was gradually decreased in intensity with the increasing amount of Pt catalyst used. Note that a physical mixture of Au and Pt nanoparticles showed a SPR peak at the same wavelength of the Au nanoparticle.[50] The gradual suppression of the SPR peak suggests that the surface of the Au nanoparticle was systematically covered with a Pt-shell mediated through a seeded-growth mechanism as demonstrated by others.[50–52] The formation of a Pt-shell on the original Au nanoparticle is reasonable given that the reduction of a Pt precursor on the surface of Au nanoparticles with a mild reducing agent is the most common method to synthesize Au-core/Pt-shell nanoparticles. For the systems described above, the nanoparticle surface obtained after crosslinking of the block copolymer ligands formed a core-shell structure through reduction during the hydrosilylation reaction. Strictly speaking, the presence of weak SPR peaks from the nanoparticles hydrosilylated with less than 200 mol % of Pt catalyst reveals that the surface of gold nanoparticles is partially covered by a Pt-shell. The presence of Pt on the surface of the Au nanoparticles was confirmed again by XPS. Fig. 5b shows the XPS spectrum of shell-crosslinked PS_{29}-*b*-I_{21}SAu_3 with the Au $4f_{7/2}$ and $4f_{5/2}$ peaks at binding energies of 84.0 and 87.6 eV and a full width at half maximum (fwhm) of 1.2 eV, characteristic peaks of Au(0), being observed.[53] In addition, the broad Pt peaks at binding energies of 71.2 and 74.6 eV in Fig. 5b suggest the presence of Pt in the shell-crosslinked Au-Pt nanoparticles. The broadening of the Pt peaks can be briefly explained by the charge transfer from Pt to sulfur and the formation of a Pt-vinyl/Pt-Si complex during the hydrosilylation reaction (Fig. SF3 for the deconvolution of Pt peaks and detailed discussion, ESI†). It should be noted that ligands making weak bonds to the core material such as tetraoctylammonium bromide or citric acid are used to facilitate the reduction of metal on the core in most cases of core-shell nanoparticle synthesis.[50–52] For the more tightly bound thiol ligands, shell formation in our method can be explained by redistribution or rearrangement of the thiol ligands trapped by the crosslinked polymer shell on the nanoparticle surface.[54,55] We expect that this method can be applied to the synthesis of a variety of core-shell nanoparticles by efficiently inhibiting aggregation of nanoparticle cores during synthesis due to the crosslinked polymeric ligands.

The availability of sub-5nm Au-Pt nanoparticles that are thermally stable to traditional processing and annealing conditions opens up a wide variety of block copolymer morphology and interfacial studies. The segregation behavior of shell-crosslinked Au-Pt nanoparticles was therefore investigated by dispersing the nanoparticles in a PS_{547}-*b*-$P2VP_{542}$ lamellar-forming diblock copolymer, which was thermally annealed at 190 °C for three days. TEM analysis reveals dark gray and white stripes corresponding to the PS and P2VP domains, respectively, (P2VP domains were stained with iodine) while the nanoparticles are observed as small black dots (Fig. 6). In contrast, Au nanoparticles without a crosslinked-shell (PS_{29}-*b*-I_{21}SAu_3) were annealed with saturated dichloromethane vapor for two days (Fig. 6a) and selective segregation near the center of the PS domains was observed. A histogram showing the distribution of nanoparticles obtained from more than 500 nanoparticles for this sample is shown in Fig. 6e. Fig. 6b is the TEM micrograph of the same composite sample from Fig. 6a after annealing with dichloromethane followed by thermal annealing at 190 °C for three days. Due to the thermal instability of Au–S bond, the nanoparticles aggregate at the center of the PS domains as shown in the magnified image in the inset. The nanoparticles merged together and formed larger particles, which are trapped in the center of the PS domains to reduce the entropic penalty caused by chain stretching.[56] PS_{29}-*b*-I_{21}SAu_4 nanoparticles without a crosslinked shell also showed a segregation behavior similar to that of PS_{29}-*b*-I_{21}SAu_3 (Fig. SF4, ESI†). Fig. 6c and d are TEM micrographs of composite samples with shell-crosslinked PS_{29}-*b*-I_{21}SAu_2 and PS_{29}-*b*-I_{21}SAu_4 in PS_{547}-*b*-$P2VP_{542}$ diblock copolymer showing a dramatic difference in segregation behavior of nanoparticles. As confirmed by the solution thermal stability test, the nanoparticles of PS_{29}-*b*-I_{21}SAu_2 were unstable in the thermally annealed PS_{547}-*b*-$P2VP_{542}$ diblock copolymer. Although the formation of nanoparticle strings (or disks) in the PS domains as seen in Fig. 6b was not observed in this case, the

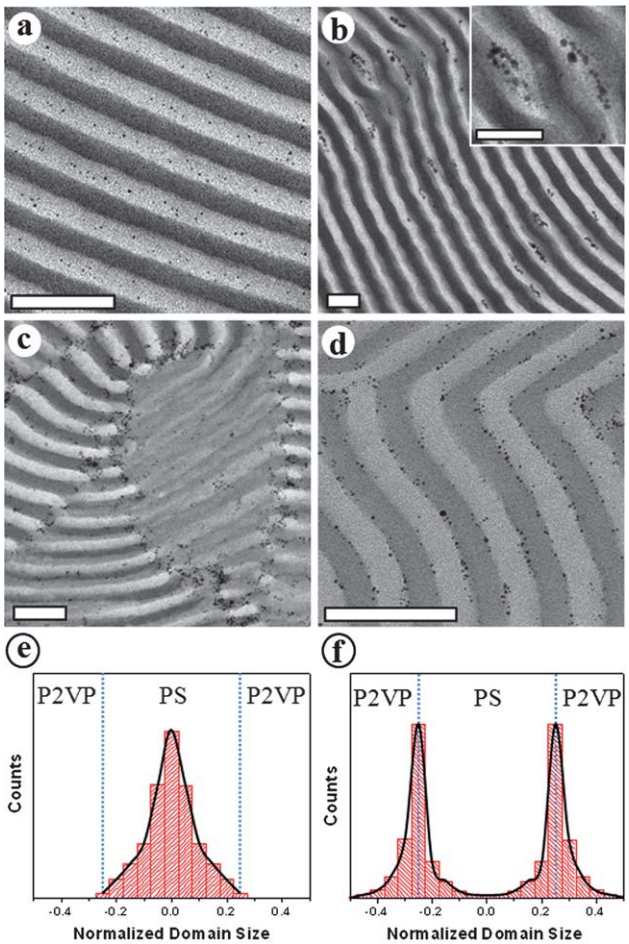

Fig. 6 Cross-sectional TEM micrographs of lamellar forming PS_{547}-*b*-$P2VP_{542}$ block copolymer (114 kg mol^{-1}) containing nanoparticles whose ligands are: (a)–(b) non-crosslinked and (c)–(d) crosslinked. The composite samples were annealed thermally under high vacuum at 190 °C for 3 days except for (a), which is solvent annealed in dichloromethane vapor. Nanoparticles used are: (a)–(b) PS_{29}-*b*-$I_{21}SAu\_3$, (c) PS_{29}-*b*-$I_{21}SAu\_2$, and (d) PS_{29}-*b*-$I_{21}SAu\_4$. Volume fractions of nanoparticles (ϕ_p) in PS_{547}-*b*-$P2VP_{542}$ are: (a)-(b) 3.5%, (c) 4.1%, (d) 4.2%. Scale bar is 100nm. (e) and (f) are histograms showing nanoparticle positions in PS_{547}-*b*-$P2VP_{542}$ microdomains obtained from the TEM micrographs in (a) and (d), respectively. The normalized domain size refers to the distance of the nanoparticle from the center of the PS domain divided by the size of a single period of the structure formed by PS_{547}-*b*-$P2VP_{542}$, and blue dotted lines located at +0.25 and −0.25 represents the interfaces between PS and P2VP. For accurate measurements, the samples were tilted to align the direction of the lamellar planes and electron beam of the microscope to reduce the broadening of interfaces caused by misalignment of the electron beam.

nanoparticles were segregated along the grain boundaries of PS_{547}-*b*-$P2VP_{542}$ microdomains (Fig. 6c). As a result of the loss of ligands from particle surface allowing P2VP to bind significantly both the Au and Pt, the nanoparticles were weakly aggregated in the P2VP domain. Then, the nanoparticles migrate subsequently to the twist and tilt grain boundaries to relieve the packing frustration of diblock copolymer chains and to swell the defects with the particle aggregates as predicted and observed previously by Bockstaller *et al.*[57] Meanwhile, the shell-crosslinked nanoparticles from PS_{29}-*b*-$I_{21}SAu\_4$ were stable without formation of nanoparticle aggregates even after thermal annealing with the nanoparticles being localized along the interface of the PS_{547}-*b*-$P2VP_{542}$ domains as shown in the TEM micrograph in Fig. 6d and in the histogram of nanoparticle distribution in the diblock copolymer domains (Fig. 6f). Considering the fact that the Au surface of nanoparticle is covered with a crosslinked network, the favorable interaction between the Au surface and the P2VP block previously reported as the main reason for the segregation of PS-coated Au nanoparticles to the interface may be significantly hindered. The localization of PS_{29}-*b*-$I_{21}SAu\_4$ nanoparticles along the interface of PS-*b*-P2VP domains may be due to the favorable interaction between P2VP block and the residual Pt catalyst in the crosslinked shell of PI block allowed by the Σ of ligands at the surface of crosslinked shell which is lower than the Σ on the nanoparticle surface. A detailed characterization and discussion will be the subject of a future paper.

Conclusions

A new synthetic strategy for the preparation of Au-core/Pt-shell (Au-Pt) nanoparticles with crosslinked polymeric ligands has been developed based on hydrosilylation of PS-*b*-PI-SH diblock copolymer ligands tethered to the Au nanoparticles. This hydrosilylation strategy offers a number of advantages compared to traditional system. First, nanoparticles with dense crosslinked shells, providing thermal stability, can be synthesized and are stable in both organic solvents at 130 °C and in a PS-*b*-P2VP block copolymer matrix annealed under vacuum at 190 °C. The thermal stability of shell-crosslinked Au-Pt nanoparticles could be tuned by varying the number of vinyl groups per polymer chain, and the number of ligands per particle. Second, reduction of the Pt catalyst during hydrosilylation leads to the formation of novel Au-Pt nanoparticles with the amount of Pt in the Au-Pt nanoparticle being controlled by the amount of catalyst used. The formation of a Pt-shell was thoroughly characterized by X-ray diffraction, high-resolution TEM, UV-VIS spectroscopy, and X-ray photoelectron spectroscopy. The ability to synthesize metallic core-shell nanoparticles stabilized with crosslinked polymeric ligands permits the segregation behavior of nanoparticles in thermally annealed block copolymer/nanoparticle composites to be studied.

Acknowledgements

This work was supported primarily by the MRSEC Program of the National Science Foundation under Award DMR05-20415. SGJ was partially supported by a Korea Research Foundation Grant funded by the Korean Government [KRF-2008-357-D00050]. We thank Dr Stephan Krämer for his help with the HR-TEM and Dr Tom Mates for his help with the XPS analysis.

References

1 M. R. Bockstaller and E. L. Thomas, *J. Phys. Chem. B*, 2003, **107**, 10017.
2 J. Y. Cheng, C. A. Ross, V. Z. H. Chan, E. L. Thomas, R. G. H. Lammertink and G. J. Vancso, *Adv. Mater.*, 2001, **13**, 1174.
3 T. F. Jaramillo, S. H. Baeck, B. R. Cuenya and E. W. McFarland, *J. Am. Chem. Soc.*, 2003, **125**, 7148.

4 S. C. Mui, P. E. Trapa, B. Huang, P. P. Soo, M. I. Lozow, T. C. Wang, R. E. Cohen, A. N. Mansour, S. Mukerjee, A. M. Mayes and D. R. Sadoway, *J. Electrochem. Soc.*, 2002, **149**, A1610.
5 S. C. Warren, L. C. Messina, L. S. Slaughter, M. Kamperman, Q. Zhou, S. M. Gruner, F. J. DiSalvo and U. Wiesner, *Science*, 2008, **320**, 1748.
6 B. Amitabh, Y. Hoichang, L. Chunzhao, C. Kilwon, B. C. Benicewicz, S. K. Kumar and L. S. Schadler, *Nat. Mater.*, 2005, **4**, 693.
7 M. R. Bockstaller, Y. Lapetnikov, S. Margel and E. L. Thomas, *J. Am. Chem. Soc.*, 2003, **125**, 5276.
8 J. J. Chiu, B. J. Kim, E. J. Kramer and D. J. Pine, *J. Am. Chem. Soc.*, 2005, **127**, 5036.
9 H. Chung, K. Ohno, T. Fukuda and R. J. Composto, *Nano Lett.*, 2005, **5**, 1878.
10 H. Kang, F. A. Detcheverry, A. N. Mangham, M. P. Stoykovich, K. C. Daoulas, R. J. Hamers, M. Muller, J. J. de Pablo and P. F. Nealey, *Phys. Rev. Lett.*, 2008, **100**, 4.
11 B. J. Kim, J. Bang, C. J. Hawker, J. J. Chiu, D. J. Pine, S. G. Jang, S. M. Yang and E. J. Kramer, *Langmuir*, 2007, **23**, 12693.
12 B. J. Kim, J. J. Chiu, G. R. Yi, D. J. Pine and E. J. Kramer, *Adv. Mater.*, 2005, **17**, 2618.
13 B. J. Kim, G. H. Fredrickson, C. J. Hawker and E. J. Kramer, *Langmuir*, 2007, **23**, 7804.
14 Q. F. Li, J. B. He, E. Glogowski, X. F. Li, J. Wang, T. Emrick and T. P. Russell, *Adv. Mater.*, 2008, **20**, 1462.
15 C. T. Lo and C. J. Chao, *Langmuir*, 2009, **25**, 12865.
16 S. Maria, A. S. Susha, M. Sommer, D. V. Talapin, A. L. Rogach and M. Thelakkat, *Macromolecules*, 2008, **41**, 6081.
17 S. W. Yeh, K. H. Wei, Y. S. Sun, U. S. Jeng and K. S. Liang, *Macromolecules*, 2003, **36**, 7903.
18 A. Noro, Y. Sageshima, S. Arai and Y. Matsushita, *Macromolecules*, 2010, **43**, 5358.
19 M. C. Daniel and D. Astruc, *Chem. Rev.*, 2004, **104**, 293.
20 J. Shan and H. Tenhu, *Chem. Commun.*, 2007, 4580.
21 B. J. Kim, G. H. Fredrickson and E. J. Kramer, *Macromolecules*, 2008, **41**, 436.
22 B. J. Kim, J. Bang, C. J. Hawker and E. J. Kramer, *Macromolecules*, 2006, **39**, 4108.
23 B. J. Kim, G. H. Fredrickson, J. Bang, C. J. Hawker and E. J. Kramer, *Macromolecules*, 2009, **42**, 6193.
24 C. D. Bain, E. B. Troughton, Y. T. Tao, J. Evall, G. M. Whitesides and R. G. Nuzzo, *J. Am. Chem. Soc.*, 1989, **111**, 321.
25 R. K. O'Reilly, C. J. Hawker and K. L. Wooley, *Chem. Soc. Rev.*, 2006, **35**, 1068.
26 M. Iijima, Y. Nagasaki, T. Okada, M. Kato and K. Kataoka, *Macromolecules*, 1999, **32**, 1140.
27 K. B. Thurmond, T. Kowalewski and K. L. Wooley, *J. Am. Chem. Soc.*, 1996, **118**, 7239.
28 X. Liu and A. Basu, *J. Am. Chem. Soc.*, 2009, **131**, 5718.
29 Y. L. Wu and J. Li, *Angew. Chem., Int. Ed.*, 2009, **48**, 3842.
30 L. Guifeng, F. Jinda, J. Rong and G. Yong, *Chem. Mater.*, 2004, **16**, 1835.
31 S. Koenig and V. Chechik, *Langmuir*, 2006, **22**, 5168.
32 X. Liu and A. Basu, *Langmuir*, 2008, **24**, 11169.
33 H. C. Dong, M. Z. Zhu, J. A. Yoon, H. F. Gao, R. C. Jin and K. Matyjaszewski, *J. Am. Chem. Soc.*, 2008, **130**, 12852.
34 M. Yoo, S. Kim, J. Lim, E. J. Kramer, C. J. Hawker, B. J. Kim and J. Bang, *Macromolecules*, 2010, **43**, 3570.
35 A. K. Roy and R. B. Taylor, *J. Am. Chem. Soc.*, 2002, **124**, 9510.
36 M. Brust, M. Walker, D. Bethell, D. J. Schiffrin and R. Whyman, *J. Chem. Soc., Chem. Commun.*, 1994, 801.
37 J. L. Speier, J. A. Webster and G. H. Barnes, *J. Am. Chem. Soc.*, 1957, **79**, 974.
38 D. J. Worsfold and S. Bywater, *Can. J. Chem.*, 1964, **42**, 2884.
39 M. J. Kade, D. J. Burke and C. J. Hawker, *J. Polym. Sci., Part A: Polym. Chem.*, 2010, **48**, 743.
40 K. Matyjaszewski and T. P. Davis, *Handbook of Radical Polymerization*, Wiley, New York, 2002.
41 J. L. Speier, R. Zimmerman and J. Webster, *J. Am. Chem. Soc.*, 1956, **78**, 2278.
42 L. N. Lewis and N. Lewis, *J. Am. Chem. Soc.*, 1986, **108**, 7228.
43 Z. Hongyu, D. Fenfang, L. Xi, Z. Bin, L. Wei and Y. Bing, *J. Phys. Chem. C*, 2008, **112**, 19360.
44 M. J. Hostetler, J. E. Wingate, C. J. Zhong, J. E. Harris, R. W. Vachet, M. R. Clark, J. D. Londono, S. J. Green, J. J. Stokes, G. D. Wignall, G. L. Glish, M. D. Porter, N. D. Evans and R. W. Murray, *Langmuir*, 1998, **14**, 17.
45 C. T. Campbell, S. C. Parker and D. E. Starr, *Science*, 2002, **298**, 811.
46 B. L. V. Prasad, S. I. Stoeva, C. M. Sorensen and K. J. Klabunde, *Chem. Mater.*, 2003, **15**, 935.
47 T. Hashimoto, M. Shibayama and H. Kawai, *Macromolecules*, 1980, **13**, 1237.
48 J. B. Xu, T. S. Zhao, Z. X. Liang and L. D. Zhu, *Chem. Mater.*, 2008, **20**, 1688.
49 K. A. Willets and R. P. Van Duyne, *Annu. Rev. Phys. Chem.*, 2007, **58**, 267.
50 M. L. Wu, D. H. Chen and T. C. Huang, *Chem. Mater.*, 2001, **13**, 599.
51 J. Luo, L. Wang, D. Mott, P. N. Njoki, Y. Lin, T. He, Z. Xu, B. N. Wanjana, I. I. S. Lim and C. J. Zhong, *Adv. Mater.*, 2008, **20**, 4342.
52 N. Kristian, Y. S. Yan and X. Wang, *Chem. Commun.*, 2008, 353.
53 J. H. Choy and Y. I. Kim, *J. Phys. Chem. B*, 2003, **107**, 3348.
54 C. Munuera and C. Ocal, *J. Chem. Phys.*, 2006, **124**, 5.
55 F. Schreiber, *Prog. Surf. Sci.*, 2000, **65**, 151.
56 R. J. Spontak, R. Shankar, M. K. Bowman, A. S. Krishnan, M. W. Hamersky, J. Samseth, M. R. Bockstaller and K. O. Rasmussen, *Nano Lett.*, 2006, **6**, 2115.
57 J. Listak and M. R. Bockstaller, *Macromolecules*, 2006, **39**, 5820.